Measurement of Quantum Turbulence in Superfluid ^{4}He

Jakub Bahyl[1]*

Supervisor: David Schmoranzer[2]†

[1] FMFI UK, Mlynská Dolina 842 48 Bratislava
[2] Katedra fyziky nízkych teplot, MFF UK, V Holešovičkách 747/2 Praha 8

Abstract: In this work we present measurements of quantum turbulence generated by an oscillating quartz tuning fork submerged in superfluid ^{4}He at various temperatures under $T_\lambda = 2.17\,\mathrm{K}$. The observed turbulent mode is quantitatively characterized by a vortex line density L, which was indirectly measured by the attenuation of second sound.

Keywords: Helium-4 · Superfluidity · Quantum turbulence · Second sound

1 Introduction to Superfluidity

As the temperature approaches absolute zero, macroscopic fluid properties can be affected by quantum phenomena. The zero temperature limit is usually followed by a solidification, but in the case of ^{3}He and ^{4}He the fluids remain in liquid state instead, which are then called *quantum fluids*.

1.1 Superfluid Helium as a Bose-Einstein Condensate

Among all basic chemical substances, helium keeps its liquid state even at absolute zero, which makes its quantum behaviour noticeable. In particular, at $T_\lambda = 2.17\mathrm{K}$ a second-order phase transition occurs and helium becomes superfluid, commonly called He-II. Due to the core composition of ^{4}He (the common helium isotope), the resulting nuclear spin equals zero. ^{4}He gas is therefore classified as a weak-interacting Bose gas. Using Bose-Einstein quantum statistics[1] can be shown that below the certain temperature ($\approx 3.15\,\mathrm{K}$ for ideal BEC and $\approx 2.17\,\mathrm{K}$ for helium) a macroscopic number of bosons occupies the lowest single quantum state.

Comparing with a classical fluid, the superfluid itself has several remarkable properties, like more than thousand times higher thermal conductivity or almost zero viscosity[2] when flowing through narrow capillaries.

In 1941 L.D. Landau proposed[3] the full phenomenological microscopic theory of thermal excitations from which the macroscopic theory (two-fluid model) of superfluid hydrodynamics can be derived.

1.2 Two-fluid Model and Second Sound

The experimental facts led Landau [4] to postulate his own theory, that under T_λ the whole helium fluid is composed of two different, almost independently behaving fluids. We recognise them as a pure *superfluid* component, which has zero viscosity, and *normal* component, obeying classical hydrodynamic laws.

These two inter-penetrating fluids are moving with their own velocity fields, denoting $\mathbf{v}_\mathrm{s}$ and $\mathbf{v}_\mathrm{n}$, and corresponding densities ρ_s, ρ_n. The total density ρ is then

$$\rho = \rho_\mathrm{s} + \rho_\mathrm{n} \tag{1}$$

and the total mass flux $\mathbf{j}$ of both components

$$\mathbf{j} = \rho_\mathrm{s}\mathbf{v}_\mathrm{s} + \rho_\mathrm{n}\mathbf{v}_\mathrm{n}\,. \tag{2}$$

According to experimental data and Landau's microscopic theory, the dependence of fractional densities on temperature is sketched below in **Figure 1**.

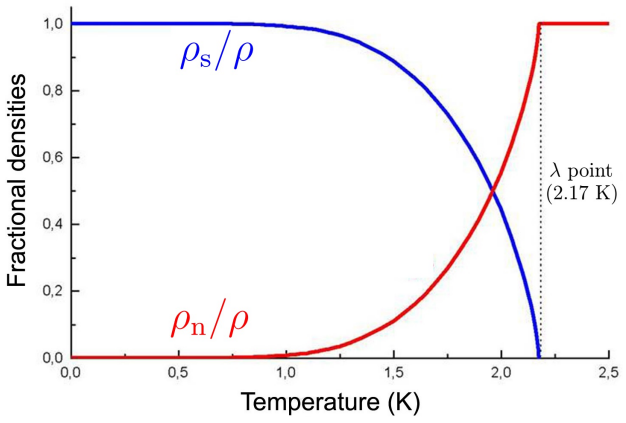

Figure 1: Temperature dependence of the normal (red) and superfluid (blue) component. The total density ρ varies only weakly with temperature.

*kubo@fks.sk
†david.schmoranzer@mff.cuni.cz

The four principal hydrodynamic equations for the two-fluid model are the laws of conservation. Assigning P as pressure, T as temperature and s as entropy per unit mass, one can derive[4] the conservation of mass, entropy and momentum for both components, respectively:

$$\frac{\partial \rho}{\partial t} + \nabla \cdot (\rho_s \mathbf{v}_s + \rho_n \mathbf{v}_n) = 0, \tag{3}$$

$$\frac{\partial (s\rho)}{\partial t} + \nabla \cdot (s\rho \mathbf{v}_n) = 0, \tag{4}$$

$$\frac{\partial \mathbf{v}_s}{\partial t} + \frac{\nabla P}{\rho} - s\nabla T = 0, \tag{5}$$

$$\frac{\partial \mathbf{v}_n}{\partial t} + \frac{\nabla P}{\rho} + \frac{\rho_s}{\rho_n} s\nabla T = 0. \tag{6}$$

This set of equations lead[5] to two wave equations. The first one for a pressure-density wave and the second one for an entropy-temperature wave:

$$\frac{\partial^2 \rho}{\partial t^2} = u_1^2 \nabla^2 \rho \qquad \frac{\partial^2 s}{\partial t^2} = u_2^2 \nabla^2 s, \tag{7}$$

in which u_1, u_2 are corresponding velocities of wave propagation

$$u_1 = \left(\frac{\partial P}{\partial \rho}\right)_s^{1/2} \qquad u_2 = \left(\frac{\rho_s}{\rho_n}\frac{Ts^2}{C_p}\right)^{1/2}, \tag{8}$$

where C_p is the specific heat. The first wave equation on the left in (7) represents ordinary sound, when both fluids oscillate identically ($\mathbf{v}_s = \mathbf{v}_n$). On the contrary, the other wave equation in (7) describes what is commonly called as *second sound*, the new wave process specific for ^{4}He, where the components oscillate in antiphase ($\rho_s \mathbf{v}_s = -\rho_n \mathbf{v}_n$). According to the continuity equation (3), for a given point the total density ρ is constant.

1.3 Quantum Effects

Since the superfluid component flows wihout dissipation, there is an analogy with electron currents in atoms. By this we have that all the superfluid atoms are connected via the macroscopic wave function of the form $\Psi = \sqrt{\rho_s/m_4}\, e^{i\phi(\mathbf{r},t)}$, where m_4 is ^{4}He core mass and $\phi(\mathbf{r},t)$ is a scalar function (phase) of coordinates and time. By applying the momentum operator $\hat{\mathbf{p}}$ it can be shown that the velocity field of superfluid component cannot make any vortices:

$$\mathrm{rot}\,\mathbf{v} = \nabla \times \frac{\hat{\mathbf{p}}|\Psi\rangle}{m_4|\Psi\rangle} = \frac{\hbar}{m_4}\nabla \times \nabla\phi(\mathbf{r},t) = \mathbf{0} \tag{9}$$

However, there is still one allowed form of rotational motion. A thin ($\approx 10^{-10}$ m wide) vortex line, whose circulation and energy density are quantized in multiples of $\kappa \approx 10^{-7}\,\mathrm{m}^2/\mathrm{s}$ and $\varepsilon_0 \approx 100\,\mathrm{eV/m}$ respectively. In the early work of Osborne[6], the basic properties of quantum vortices were studied in rotating container filled with superfluid ^{4}He. In this case, the vortices are fully polarized and form hexagonal structure. Generally in considerably complex situations, the vortices may be disordered and unpolarized. Thus for an isotropic and homogeneous distribution one can define L as the total length of vortex lines located in unit volume.

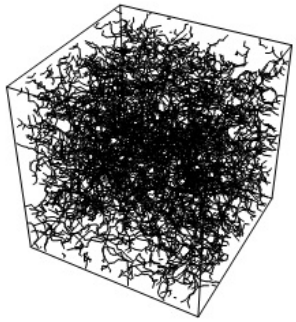

Figure 2: A numeric simulation of randomly distributed vortex lines.

2 Quantum Turbulence

The two-fluid nature of superfluid ^{4}He definitely provides a more general form of motion of quantum fluids. Consequently, the understanding of such a remarkable physical system as quantum turbulence (QT), may turn to a deeper understanding of turbulence in classical fluids, which is, till this day, far from complete.

2.1 Effect of QT on Attenuation of Propagating Second Sound Wave

Strictly speaking, it is not true that the superfluid and normal components act independently of each other. They are connected (due to the weak interaction between helium atoms) through the *mutual friction force*. A formula for this force was derived by Vinen and Hall, based on experimental data[7]

$$\mathbf{F}_{sn} = B\frac{\rho_n \rho_s}{\rho}\hat{\Omega} \times [\Omega \times (\mathbf{v}_n - \mathbf{v}_s)] + B'\frac{\rho_n \rho_s}{\rho}[\Omega \times (\mathbf{v}_n - \mathbf{v}_s)], \tag{10}$$

where Ω stands for the local vorticity of normal component, $\hat{\Omega}$ for its normalised vector and B, B' are temperature dependent coefficients.

From equation (10), it is clear that when the second sound wave $\mathbf{v}_{ns} = \mathbf{v}_n - \mathbf{v}_s$ is passing through the system of quantum vortices, the first force term with B would suppress it. This leads to linear resistance and therefore to an exponential attenuation of second sound amplitude. The second term with B' is perpendicular to $\mathbf{v}_{ns}$, so there is no dissipation of energy.

If we choose the $\mathbf{z}$-axis as the direction of propagating second sound wave, using the formula for mutual friction force (10) the corresponding wave equation takes the form [8]

$$\frac{\partial^2 \mathbf{v}_{ns}}{\partial^2 z} - \frac{B\kappa L}{3u_2^2}\frac{\partial \mathbf{v}_{ns}}{\partial t} - \frac{1}{u_2^2}\frac{\partial^2 \mathbf{v}_{ns}}{\partial^2 t} = 0. \qquad (11)$$

Here we find the solution in the expected form of exponentially attenuated wave $v_{ns} \propto \exp(-\alpha z)$ with the attenuation constant $\alpha = B\kappa L/6u_2$.

Of course, mutual friction force is not the only dissipative effect. While any amount of normal component is still present, classical viscous damping acts even if no QT is created. Thus the resonance peak of second sound signal generated in a finite system (resonator) has a non-zero width Δf_0 when no vortices are present. As we start to produce QT, the peak will broaden and the amplitude will decrease.

Measuring the initial peak height A_0, initial resonance width Δf_0 and decreased height A provides a sufficient amount of information to determine[8] the vortex line density L, in particular

$$L = \frac{6\pi\Delta f_0}{B\kappa}\left(\frac{A_0}{A} - 1\right). \qquad (12)$$

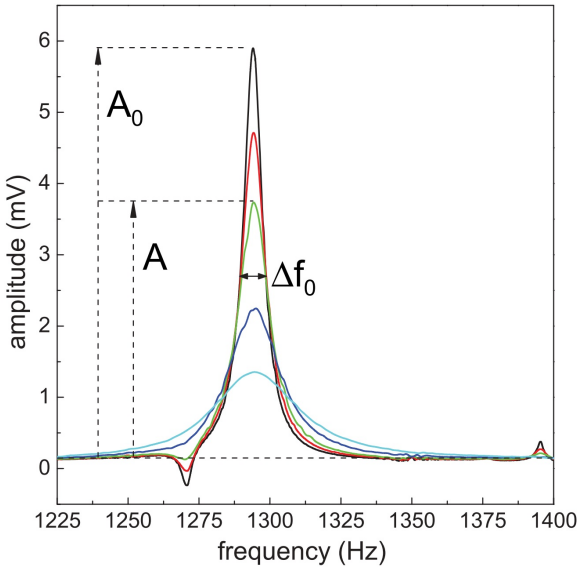

Figure 3: An example of observed attenuated second sound signal. Data source:[9].

3 Experimental Setup

The whole system consisting of QT generator and two second sound sensors was placed into a cylindrical resonator cavity of diameter $d = 10\,\text{mm}$ and height $H = 54\,\text{mm}$, as shown in **Figure 4**. One of the second sound sensors (speaker) is connected to the waveform generator and the other one (receiver) to a SR-830 lock-in amplifier. A more detailed description is presented later in this chapter.

Generation of QT is ensured by an oscillating quartz tuning fork, located in the middle of the resonator. Two second sound sensors (source and detector) have been implemented at the ends of the resonator, facing each other. The resonator itself is not enclosed entirely - a small 1mm thin hole is drilled through the body, connecting the cavity to the open superfluid helium bath.

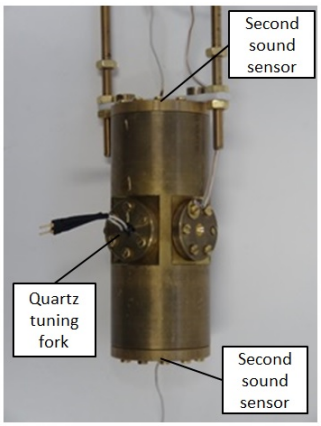

Figure 4: Photo of the resonator used in experiment.

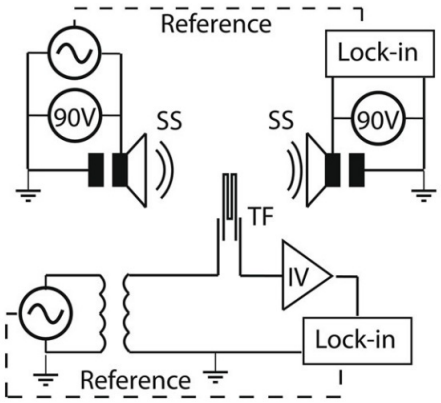

Figure 5: Electrical schematics of the setup.

3.1 Quartz Tuning Fork

In general, quartz tuning forks are well-known commercially produced piezoelectric oscillators because of their wide application as a frequency standards in watches. In our work we used an unconventional fork with fundamental resonance at 6.5 kHz (in vacuum). Geometry of the fork is sketched in **Figure 6**.

The fork's size is given by prong length $L = 35\,\mathrm{mm}$, prong width $W = 75\mu\mathrm{m}$, thickness $T = 90\mu\mathrm{m}$ and the distance between prongs $D = 90\mu\mathrm{m}$. The fork was driven by an amplified alternating voltage $U \propto e^{i\omega t}$, causing the anti-phase lateral oscillation of fork's prongs. The first flexural overtone can be found at the frequency $f_1 = 40\,\mathrm{kHz}$. Two other important properties of the fork are the effective mass of one prong m_{eff} and a fork constant a. For our case, we can estimate them (using formulas and data from [10, 11]) as:

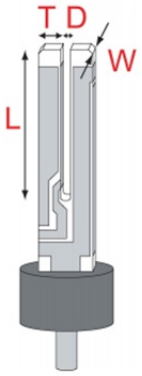

Figure 6: Sketch of quartz tuning fork.

$$m_{\mathrm{eff}} = \frac{1}{4} LTV\rho_q = 1.52 \cdot 10^{-8}\,\mathrm{kg},$$
$$a_{\mathrm{fund}} = 3.61 \cdot 10^{-7}\,\mathrm{Cm}^{-1},$$
$$a_{\mathrm{over}} = 1.38 \cdot 10^{-6}\,\mathrm{Cm}^{-1},$$

where $\rho_q = 2650\,\mathrm{kg/m^3}$ is the quartz density. Values of the fork constants were taken from[11], where tuning forks of the same parameters and from the same series were used.

It was also shown[10] that by applying AC voltage with amplitude U_A results in a driving force acting on the fork's prongs of magnitude $F = \frac{1}{2}aU$. Moreover, by measuring the current response I we can determine the velocity at the tip of the prongs as $v = I/a$. Knowledge of these parameters is crucial for all measurements related with superfluid hydrodynamics.

3.2 Second Sound Source and Detector

Second sound is a wave of temperature and entropy, but can be produced purely mechanically. In particular, when a semi-permeable membrane with submicron pores is oscillating in He-II, the superfluid component can flow through the pores much easier than the normal component (due to the lack of viscosity). Thus, its oscillation will push only the normal component and consequently, this creates (due to continuity equations) a local oscillation of densities ρ_{n}, ρ_{s} and hence, a longitudinal wave of second sound. At the right frequency of oscillation, this results in a resonant second-sound standing wave in the experimental cylindrical cavity.

In our experiment we used two identical sensor devices to produce and also detect the second sound. The sensor itself is essentially a capacitor where one electrode consists of the membrane with a 100 nm thick gold layer above the surface and the other electrode is made of brass. The full sketch and photo can be seen in **Figure 7**.

The gold electrode is electrically connected with the resonator body while the other electrode to the wave generator or lock-in amplifier (depends whether the device is set as a speaker or receiver). Together, these electrodes form a capacitor of $\approx 60 - 100\,\mathrm{pF}$ and applying an AC voltage (units of Volts) superimposed on a 90 V DC bias causes the oscillation of the membrane and therefore production of second sound.

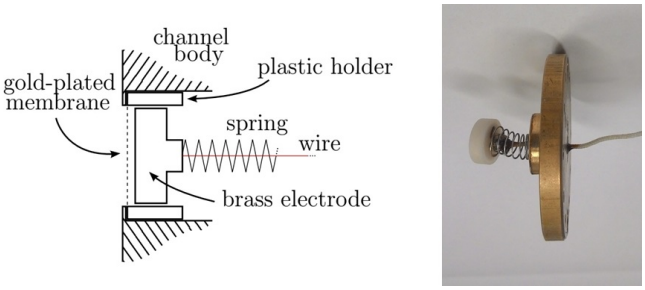

Figure 7: Left: Technical sketch showing the parts of the second sound sensor. Right: A photograph of our construction.

Because of finite distance between the sensors H, we observe many harmonic resonance modes. The resonance frequency can be estimated from the equation for standing waves: $f = \frac{u_2}{\lambda} = \frac{u_2}{2H}n$, where n is a positive integer.

3.3 Reaching Low Temperatures

The resonator with all important devices were put into a vessel, designed for working with cryogenic fluids. At the top, the cryostat allows access into the helium bath, but at the same time, the cryostat must be well-insulated from external heat fluxes.

After the cryostat was pre-cooled to liquid nitrogen (LN_2) temperature ($\approx 77\,\mathrm{K}$), we continued precooling with helium vapour and finally transferred liquid helium (LHe) at ($\approx 4.2\,\mathrm{K}$) from a transport dewar. Vapours from the rapidly evaporating LHe were immediately pumped by a set of Roots-pumps so that the inner pressure above the LHe surface was further decreased. Reducing the saturated vapour pressure provided the cooling even below T_λ. This method works efficiently until the minimum temperature of $\approx 1.25\,\mathrm{K}$ is reached.

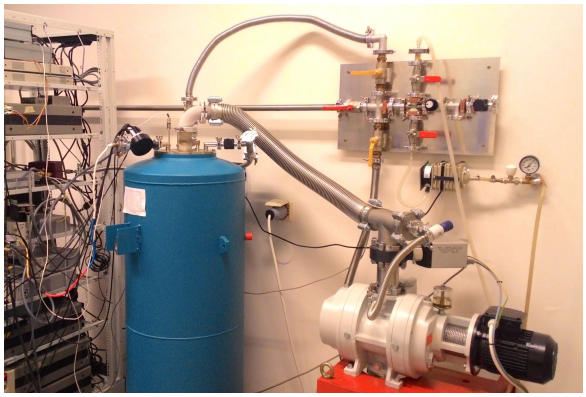

Figure 8: Photograph of the experimental setup - Left: cryostat, pipes where helium gas is flowing out of the system. Right: Roots-pump.

During the measurements it was crucial to have the temperature stabilized minimal deviations. Two methods have been used for measuring the temperature. The first was a direct resistance measurement of a miniature semiconductor thermometer (Germanium thin film on GaAs substrate) placed in the helium bath, with calibration known from previous experiments. The second method was a simple conversion between saturated vapour pressure and temperature based on [12]. The pressure was regulated (both manually and electronically) by manipulating the pump valve.

To summarize, we prepared a cooling system able to reach any temperature above $\approx 1.25\,\mathrm{K}$.

Overall, we did systematic measurements at 6 different temperatures: 2.15 K, 2.05 K, 1.95 K, 1.80 K, 1.55 K, 1.35 K. Although our total experimental temperature range is less than 1 K, there are dramatical changes in the composition of LHe within this interval. One can recall (graph in **Figure 1**) that at 2.15 K there is only about 5% of the superfluid component, but at 1.35 K it is more than 90%.

Figure 9 shows the time trace of the temperature inside the cell. Temperatures below $\approx 1.30\,\mathrm{K}$ were not stable, so the lowest fixed value was set to 1.35 K.

4 Measurement Methods

The distance between the speaker and receiver is $H = 54\,\mathrm{mm}$ and the second sound velocity is approximately $u_2 \approx 20\,\mathrm{m/s}$ within the range of temperatures $(1.35\,\mathrm{K} - 1.95\,\mathrm{K})$. In *frequency sweep mode* the second sound speaker was oscillating with a frequency that was changing along some chosen range. This was important for characterizing the modes of resonance with thee frequencies f_0^n, widths Δf^n, signal amplitude U_0 and background signal (offset) U_{off}.

The observed 1$^{\mathrm{st}}$resonance mode frequency was found to be $\approx 200\,\mathrm{Hz}$. Additionally, this mode is most sensitive in the middle of resonator, where the fork is located. Therefore, all the measurements including second sound were made at the 1$^{\mathrm{st}}$ mode.

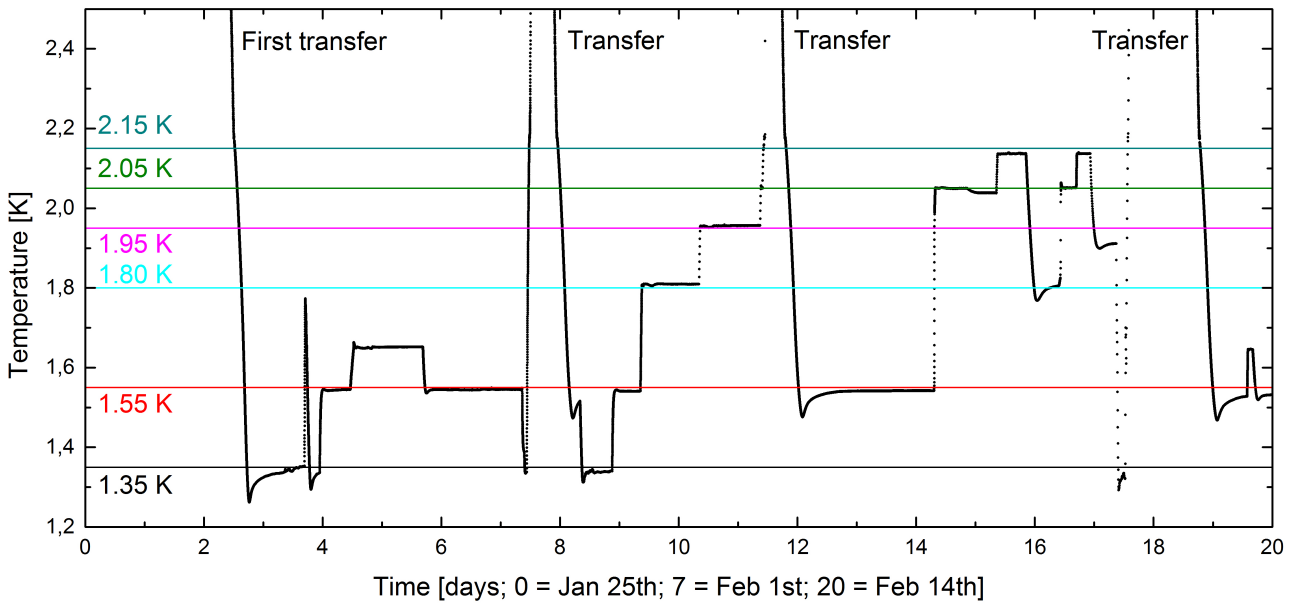

Figure 9: Record of the temperature inside the cryostat. Due to strong evaporation of superfluid helium and relatively long durations of the measurements at each temperature, we had to refill the cryostat three times.

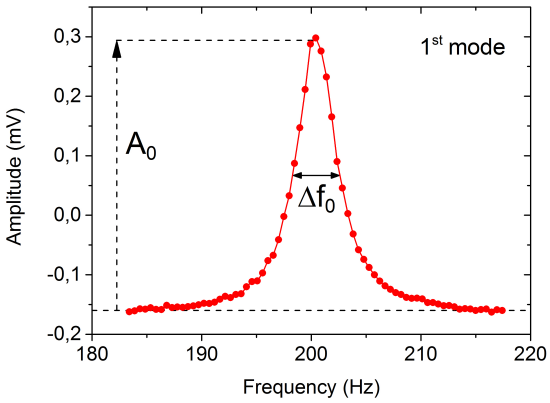

Figure 10: 1st harmonic mode of second sound. Peak height A_0 and width Δf_0 are important parameters when inferring the vortex line density.

The fitted full line is a Lorentzian curve with the general formula from [10]:

$$U(\omega) = U_{\text{off}} + U_0 \frac{(\Delta\omega)^2\omega^2}{(\omega^2 - \omega_0^2)^2 + (\Delta\omega)^2\omega^2}. \quad (13)$$

Next, in *constant drive mode*, the second sound ran continuously on its 1st resonance mode whilst the fork oscillated also at its resonance (fundamental or overtone). It has already been shown that an object oscillating with sufficient velocity can produce quantized vortices in superfluid helium. For this purpose, we used the tuning fork mounted in the second sound resonator. Our measurement protocol is given in the following steps:

1) First, after the desired temperature in the cryostat has been reached, we run the frequency sweep on tuning fork and second sound independently. The tuning fork frequency sweeps are repeated at different drive levels. This gives us the necessary information about the resonance frequencies and widths.

2) Next we set up the second sound sensors in constant drive mode at its fundamental resonance and allow up to 3 minutes for stabilization.

3) When this time has passed, we also run the tuning fork in constant drive mode at its resonance (fundamental or overtone) with a given voltage amplitude U_0 for 3 minutes.

4) The tuning fork is subsequently turned off and the second sound is again left to stabilize for 2 minutes.

5) The values of A and A_0 were taken as averages of the periods when the tuning fork was on and off, respectively (see **Figure 11**).

The five aforementioned steps were repeated for several values of voltage applied across the tuning fork, for both fundamental and overtone mode at all six temperatures. We have always proceeded from low values of driving voltage to higher ones gradually, so that it is clear, at which point any measurable amount of quantum vortices appears.

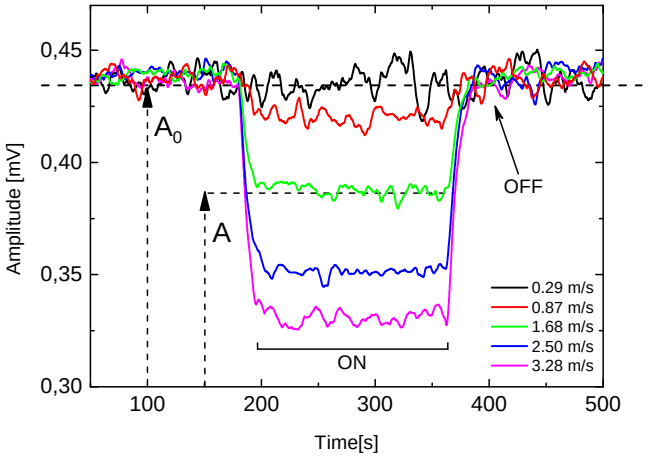

Figure 11: An example of second sound attenuation due to the presence of quantized vortices, produced by an oscillating tuning fork at various velocities. "ON" and "OFF" labels describe the state of the tuning fork. The time on the x-axis is measured from the beginning of each particular run. Values shown in this graph are taken at the temperature $T = 1.95\,\text{K}$. The measurement at the velocity of $0.29\,\text{m/s}$ corresponds to a vortex line density $L_0 = 3 \times 10^6\,\text{m}^{-2}$ and is taken as an estimate of the sensitivity threshold of our measurement technique.

By collecting datasets of A, A_0 and Δf_0 we could estimate the vortex line density L:

$$L = \frac{6\pi\Delta f_0}{B\kappa}\left(\frac{A_0}{A} - 1\right), \quad (14)$$

and the fork tip velocity $v = I/a$, where I is current response and a the fork constant. The resulting plot (**Figure 12**) is shown in the next page.

We should point out that the results for L as derived in **Section 2.1** are valid only for homogeneously and isotropically distributed vortices. The amount of quantized vortices is expected to be higher near the fork than further away from it. Since we utilized the 1st second sound resonant mode, we have, in fact, measured the 1st Fourier component of the vortex line density spatial distribution[13]. This is sufficient for the purposes of (roughly) estimating the quantities

of quantized vortices produced, but the true values of L near the tuning fork may differ by some factor and could be obtained only by measurements using several additional second sound resonant modes.

5 Results

Here we present the experimental data obtained from the measurements of quantum turbulence. The tuning fork has been immersed in superfluid ^{4}He and forced to oscillate at two, geometrically different (in the sense of different velocity profile along the fork's prongs) modes - *fundamental* [6380 Hz] and *overtone* [40000 Hz]. This chapter is focused on the measurement of vortex line density L (total length of vortices in unit volume) using the second sound attenuation technique. We will try to find the conditions for production of quantized vortices and also, quantify their amount.

From **Figure 12** we observe that no significant amounts of vortex lines are produced before a certain critical velocity is exceeded. Furthermore, we find that the amount of quantized vortices produced is temperature-independent and scales only with the velocity of the tuning fork.

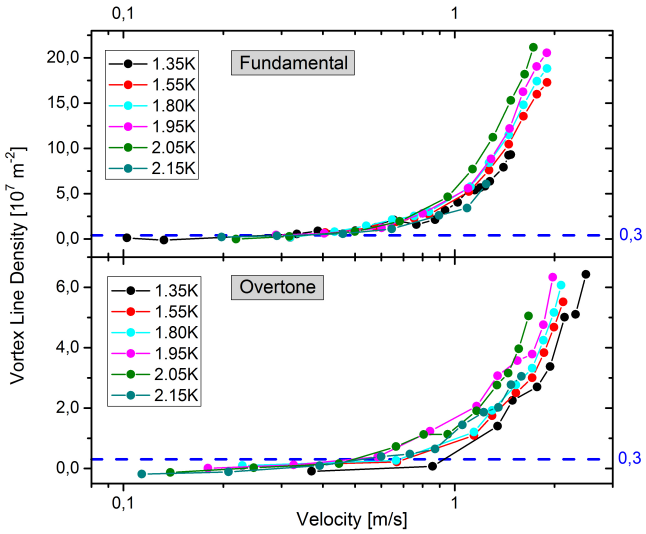

Figure 12: Vortex line density L against the (logarithmically scaled) peak velocity of the tuning fork v. The *blue dotted line* marks the threshold level $L_0 \approx 3 \cdot 10^6\,\mathrm{m}^{-2}$ introduced in **Figure 3.2**, above which the measured vortex line density can be regarded as reliable.

Plotting L on a logarithmic scale we observe (see **Figure 13**) that the critical velocities, above which the quantum vortices are produced in much larger amounts, are also independent of temperature. Bearing in mind the sensitivity threshold, we estimate these critical velocities for the fundamental and overtone modes to be $v_c^f = 0.3 \pm 0.1\,\mathrm{m/s}$, and $v_c^o = 0.7 \pm 0.2\,\mathrm{m/s}$, respectively. Moreover, the critical velocity is expected to scale with frequency as $\propto \sqrt{\kappa\omega}$[14], where ω is angular frequency and κ the circulation quantum. From our results we get $v_c^f/v_c^o \cdot \sqrt{f_0^o/f_0^f} \doteq 1.06$, which is consistent with the given scaling.

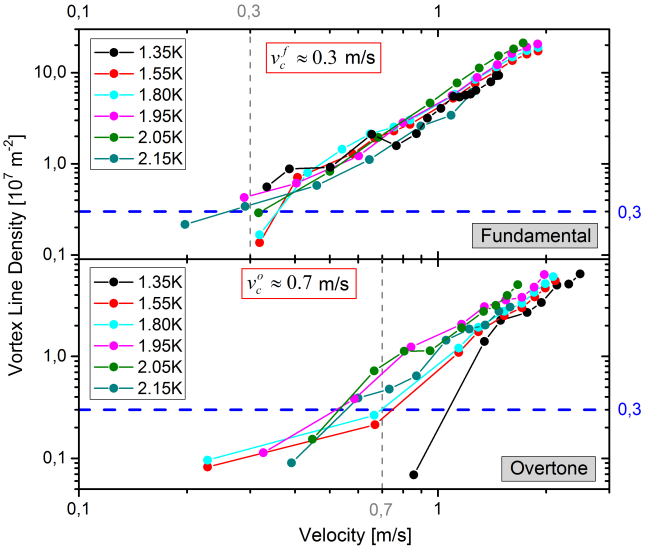

Figure 13: Log-log graph of the vortex line density L against the peak velocity of the tuning fork (the same data as in **Figure 11**). This graph better illustrates the position of threshold $L_0 \approx 3 \cdot 10^6\,\mathrm{m}^{-2}$ (*blue dashed lines*) and the temperature-independent critical velocities (*grey dashed lines*). The tuning fork peak velocity is determined with an uncertainty of about 10% that arises from the electrical calibration procedure. The vortex line density is affected by a systematic error that is mainly due to the assumption of a homogeneous isotropic tangle in deriving (14) that obviously does not correspond to the vortex tangle produced in the vicinity of the tuning fork.

Increasing the sensitivity of the second sound measurement (and thus lowering the threshold level) would allow determining the critical velocities with better accuracy and reduce the scatter in the observed data. Although the design of the second sound resonator and sensors is far from perfect, the current sensitivity is sufficient for a qualitative discussion of the relationship between the obtained vortex line densities and the drag forces acting on the tuning fork.

6 Conclusions

In this work, we have shown data reflecting the tuning fork oscillations in superfluid ^{4}He bath (at six different velocities - $1.35\,\mathrm{K}$, $1.55\,\mathrm{K}$, $1.80\,\mathrm{K}$, $1.95\,\mathrm{K}$, $2.05\,\mathrm{K}$, $2.15\,\mathrm{K}$ - as well as the second sound waves propagating through the resonator. The method of second sound attenuation showed that the only relevant parameter related with production of quantized vortices is the velocity amplitude of the fork tip and the (high enough) frequency of oscillation. We estimated the critical velocities for the fundamental and overtone modes to be $v_c^f = 0.3 \pm 0.1\,\mathrm{m/s}$, and $v_c^o = 0.7 \pm 0.2\,\mathrm{m/s}$, respectively, which should scale with the frequency as $\propto \sqrt{\kappa\omega}$. We also confirmed that this scaling is consistent with the obtained critical velocities.

The results contained within this work could be used in further research of quantum hydrodynamics where the fork's data would be studied more precisely. Till these days, it is not yet clear if the quantum turbulence of superfluid component is somehow connected with the classical turbulence of normal component. During this experiment we measured a large quantity of data characterising the behaviour of the tuning fork through the applied force and resulting velocity. The most general assumption is the existence of two critical velocities, one for classical turbulence and second for QT. Comparing the data calculated for the vortex line density in this work with the hydrodynamic data hidden in measured forces and velocities could help to find the final answer.

References

[1] TONG, D. *Statistical physics*. University of Cambridge

[2] TISZA, L. *The viscosity of liquid helium and the Bose-Einstein statistics. Comptes Rendus Acad. Sciences*, 207:1186-1189, 1952.

[3] LANDAU, L.D. *The theory of superfluidity of helium II* J. Phys. USSR, Vol. 11, 91 (1947)

[4] LANDAU, L.D. and LIFSHITZ, E.M. *Fluid Mechanics*. Second English Edition. Pergamon Books Ltd., 1987. ISBN 0-08-033933-6.

[5] SKRBEK, L. et al. *Fyzika nízkých teplot*. 1. vydání. Praha: *MatfyzPress*, 2011. ISBN 978-80-7378-168-2.

[6] OSBORNE, D.V. *The Rotation of Liquid Helium-II* Proc. of the Royal Soc. London Series A, 63(368): 909-912, 1950.

[7] VINEN, W.F. and HALL, H.E. *The theory of mutual friction in uniformly rotating helium II*. Proc. Royal Soc. London 238 (1957) 204

[8] VARGA, E. *Second sound as a tool to study He-II flow* Bachelor thesis, 2012.

[9] S. BABUIN, M. STAMMEIER, E. VARGA, M. ROTTER, L. SKRBEK *Quantum turbulence of bellows-driven* ^{4}He *superflow: Steady state* Phys. Rev. B, 86, 2012

[10] R. BLAAUWGEERS and col. *Quartz tuning fork: Thermometer, Pressure- and Viscometer for Helium Liquids* Journal of low. temp. phys., Vol. 146, 2007

[11] R.I. BRADLEYS, D. SCHMORANZER and col. *Crossover from hydrodynamic to acoustic drag on quartz tuning forks in normal and superfluid* ^{4}He. Phys. Rev. B, **85** (2012)

[12] DONNELLY, R.J., BARENGHI, C.F *The Observed Properties of Liquid Helium at the Saturated Vapor Pressure*. American Ins. of Phys. and Chem. Soc. (1998)

[13] VARGA, E., BABUIN, S., SKRBEK, L. *Second-sound studies of coflow and counterflow of superfluid* ^{4}He *in channels*. Physics of fluids **27** (2015)

[14] R. HÄNNINEN, W. SCHOEPE *Dynamical Scaling of the Critical Velocity for the Onset of Turbulence in Oscillatory Superflows*. J. Low Temp. Phys. **164**: 1-4 (2011)